

Isoindolinedione-Benzamide Pyridinium Derivatives for Targeting Alzheimer's Disease

Milad Noori, Mino Khalili Ghomi, Navid Dastyafteh, Najmeh Oliyaei, Haleh Hamedifar, Shahrzad Javanshir, Nader Tanideh, Elahe Sattarinezhad, Fateme Sattari, Masoud Haghani, Hojjat Rahmani, Bagher Larijani, Mohammad Mahdavi, Mir H. Hajimiri,* and Aida Irajii*



Cite This: *ACS Omega* 2024, 9, 48032–48043



Read Online

ACCESS |



Metrics & More

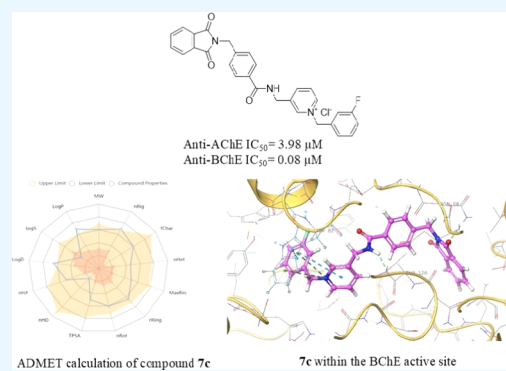


Article Recommendations



Supporting Information

ABSTRACT: An Isoindolinedione-benzamide pyridinium derivatives were designed through a structure-based strategy and synthesized as novel multifunctional anti-Alzheimer agents. The inhibitory activities of all 17 derivatives against acetylcholinesterase and butyrylcholinesterase were evaluated. Results exhibited that compound 7j displayed promising AChE inhibitory activity with an IC_{50} value of $0.26 \pm 0.07 \mu M$, and compound 7c exhibited an IC_{50} value of $0.08 \pm 0.01 \mu M$ against BChE with 132-fold better inhibitory activity in comparison with positive control. Next, the enzyme kinetics studies and detailed binding mode via molecular docking were performed for the most potent compounds. Additionally, molecular dynamics simulations were accomplished to further investigate the potent compound's interaction, orientation, and conformation over the related enzymes. The neurotoxicity of the most potent derivative was executed against SH-SY5Y, and the mRNA levels of GSK-3 α and GSK-3 β after treatment with 7c on SH-SY5Y were evaluated. Results exhibited the mRNA levels of GSK-3 β were decreased compared to the control group. All these results indicate that 7c is a good starting point for developing a multifunctional anti-Alzheimer compound.



1. INTRODUCTION

Alzheimer's disease (AD) is a neurodegenerative disorder characterized by losing memory and cognitive functions. Worldwide, it is estimated that 55 million people have dementia, and this number is still growing and is expected to increase to 153 million by 2050.¹

The major pathological changes associated with AD include the extensive loss of neurons accompanied by a progressive decline in the acetylcholine (ACh) level known as cholinergic dysfunction, extracellular deposits of senile plaques, and intracellular formation of the neurofibrillary tangle. Several other critical factors are involved in the pathogenesis of AD, including oxidative stress, metal dyshomeostasis, inflammation, and mitochondrial dysfunction.^{2–4}

According to cholinergic dysfunction. Acetylcholinesterase (AChE) catalyzes the neurotransmitter ACh hydrolysis into acetic acid and choline. AChE is located at all cholinergic sites, predominantly at the postsynaptic neuromuscular junction, and catalyzes the breakdown, hydrolysis, and inactivation of ACh, thereby controlling its amount in the synapse.^{5,6} Butyrylcholinesterase (BChE) is another ChE in the central and peripheral nervous systems. Several studies have demonstrated that the level of BChE increases in several specific brain regions, probably to offset the role of AChE at the late stage of the disease when the level of AChE decreases.⁷

Thus, inhibition of cholinesterase (ChE) enzymes would increase the levels of ACh in AD patients and improve cognitive impairment.⁸ Crystallographic studies revealed that ChE has two binding sites: the active site at the bottom of a deep narrow 20 Å gorge with the catalytic triad and the anionic subsite called the catalytic active site (CAS) and the peripheral anionic site (PAS) near the entrance of the gorge. PAS was originally thought to include multiple negatively charged amino acids and as a result, cationic ligands have a high affinity toward this pocket and this interaction lead to the catalysis of ACh hydrolysis in cholinergic synapses.^{9,10}

Glycogen synthase kinase 3 (GSK3) is a serine-threonine kinase that phosphorylates several brain proteins, including amyloid precursor protein (APP), neurofilaments, and the microtubule-associated protein Tau, resulting in the formation of toxic A β plaque and neurofibril tangles.^{11,12} There are two highly conserved isoforms of GSK3: GSK-3 α and GSK-3 β . In patients with AD, there is evidence of increased expression of

Received: May 4, 2024

Revised: October 26, 2024

Accepted: November 5, 2024

Published: November 25, 2024



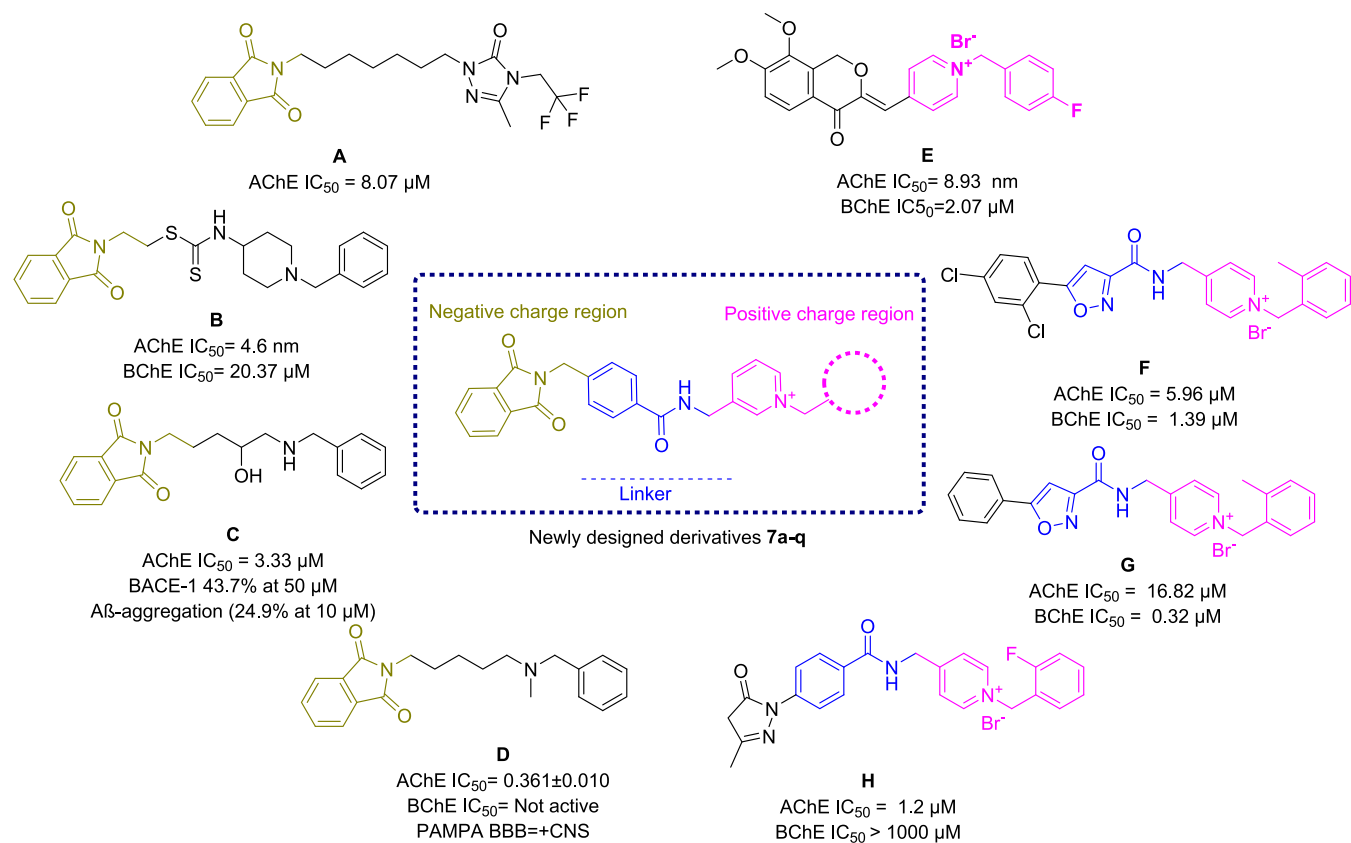


Figure 1. Design strategy of new isoindolinedione bearing benzamide pyridinium derivatives according to previously reported AChE and BChE inhibitors (A–H).

GSK-3 β , and in animal and *in vitro* models of AD, GSK-3 β appears to be associated with biological mechanisms that lead to pro-inflammatory, the formation of senile plaques and neurofibrillary tangles.¹³ The overexpression of GSK-3 β in transgenic mice is linked with many neuropathologic features. GSK3 α has been shown to regulate APP cleavage resulting in the increased production of A β .¹⁴ It was confirmed that the reduced level of GSK-3 β led to improve cognition, axonal transport, and impairment linked to alleviate neurodegenerative diseases.¹⁵

Current drug FDA-approved therapy for AD is based on restoring cholinergic activity using ChE inhibitors, including donepezil, rivastigmine, and galantamine. These drugs do not prevent or treat the neurodegenerative processes and offer symptomatic treatment with improving cognition and memory.¹⁶ AD requires a novel therapy because the available treatment is insufficient and requires considering different aspects of the disease. Notably, recent approvals in the USA include anti-amyloid monoclonal antibodies such as lecanemab and aducanumab and these medications slow clinical decline by intervening in the fundamental biological processes underlying the disease.¹⁷

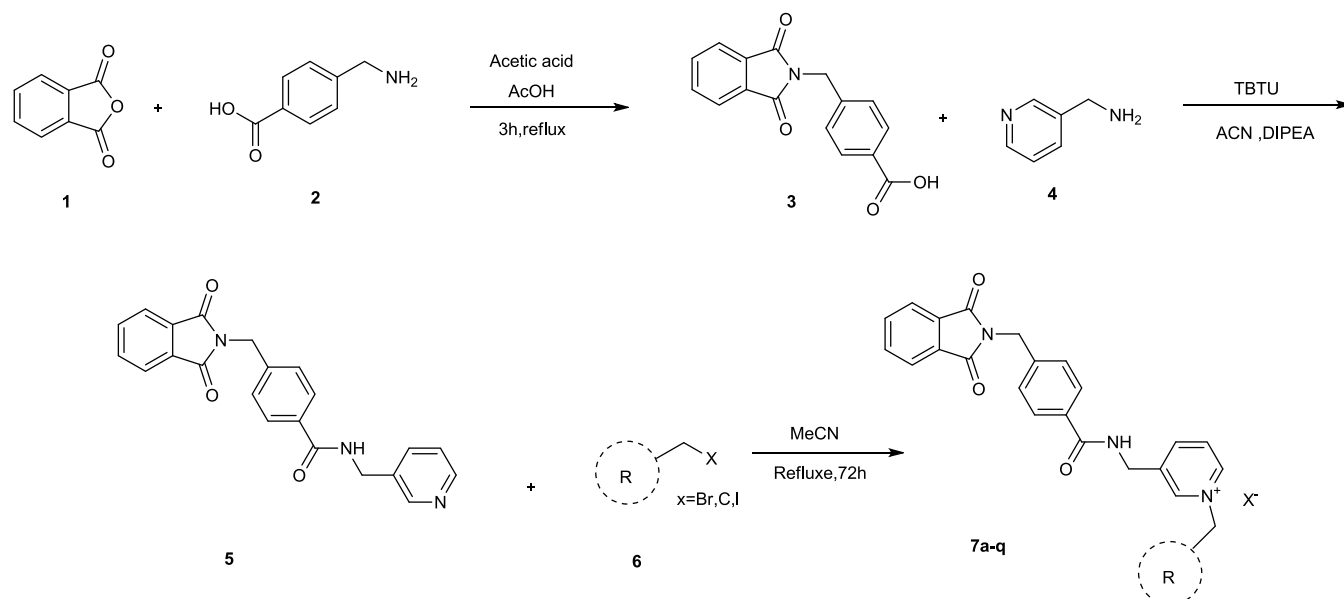
In the pursuit of developing novel therapeutic agents for AD, the rational design of molecules is fundamental. Heterocyclic compounds, such as those containing phthalimide and isoindolinedione moieties, have garnered significant attention in medicinal chemistry due to their potential as ChE inhibitors.^{18–21} Notably, pyridinium hybrids and N-arylpyridinium-based derivatives have demonstrated promising inhibitory activity against both AChE and BChE.^{22–24} As a result, we present the design, synthesis, and biological

evaluation of a novel series of isoindoline-1,3-dione derivatives bearing benzamide pyridinium, 7a–q, as potential ChE inhibitors for systematic treatment and improving cognition and memory. Molecular docking, molecular dynamics, and kinetic studies of the most potent analog were performed. We also tested the neurotoxicity of the most active derivative against the SH-SY5Y cell line. Furthermore, the present results provide a novel perspective on the level of GSK-3 α and GSK-3 β mRNAs in the neuronal cell after the treatment with potent derivatives to target the pathway of disease and hinder the progression of AD.

2. RESULTS AND DISCUSSION

2.1. Designing. Heterocycles, which contain at least one heteroatom such as nitrogen, oxygen, or sulfur, play a crucial role in medicinal chemistry as cholinesterase inhibitors.^{25,26} Phthalimide, isoindoline-1,3-dione, and their structurally related heterocycles analogs represent a class of compounds utilized in the search for novel hit or lead compounds as ChE inhibitors, owing to their distinctive structural features. Its carbonyl groups might facilitate hydrogen bonding with the target residue, and its aromatic ring probably participates in different hydrophobic interactions with its target. In 2019, phthalimide heterodimers endowed with 1,2,4-triazolin-3-one were developed with different lengths of carbons from 2 to 10. It was concluded that the length of the linker plays the most critical role in the potency, and compound A (Figure 1), as a dual binding site inhibitor, recorded an IC₅₀ value of 8.07 μM against AChE.²⁷ Phthalimide-dithiocarbamate hybrid is another example, and the most potent derivative displayed satisfactory potency against AChE and BChE. Molecular

Scheme 1. Synthesis of Isoindoline-1,3-dione Derivatives, 7a–q



docking of **B** exhibited H-bond and hydrophobic interactions with Ser293 and Phe338 (acyl-binding pocket of CAS) with phthalimide moiety in the AChE active site.²¹ Compound **C** as a noncompetitive inhibitor²⁰ and compound **D** as a potent AChE and BACE1 inhibitor¹⁹ bearing phthalimide moiety are other AChE inhibitors. Recently, isoindolinedione-pyridinium hybrids were developed and tested against AChE and exhibited IC_{50} values ranging from 2.1 to 7.4 μM . Notably, *para*-fluoro substituted compounds emerged as particularly significant due to their ability to effectively target the small-sized AChE binding site.¹⁸ This observation might partially explain the significant inhibitory of phthalimide moiety as the anti-ChE agent.

N-arylpyridinium-based derivatives also get considerable attention in modern medicinal chemistry, exhibiting AChE and BChE inhibitory activity. Starting from this moiety, donepezil is an oral drug with ChE inhibitory potency as an anti-AD drug. It was shown that the benzylpiperidine part of the drug occupies CAS while inden-1-one moiety oriented toward the PAS pocket. In a previous investigation, 4-isochromanone hybrids bearing N-benzylpyridinium moiety (**E**) as dual binding site AChE inhibitor exhibited high AChE/BChE selectivity ($SI > 230$) with IC_{50} value of 8.93 nM. Kinetic and molecular modeling studies proposed mixed-type inhibition with simultaneous binding to CAS and PAS of AChE.²² In another attempt to develop a potent ChE inhibitor N-benzylpyridinium moiety linked to arylisoxazole derivatives (**F** and **G**) was developed as a selective BChE inhibitor with IC_{50} in the range of 0.32 ± 0.06 to $17.82 \pm 0.38 \mu\text{M}$ against BChE and 5.96 ± 0.41 to $97.93 \pm 0.61 \mu\text{M}$ against AChE.²³ In another study, edaravone was conjugated to N-benzylpyridinium moiety, and interestingly significant *in vitro* AChE inhibitory activities were observed ($IC_{50} = 1.2\text{--}4.6 \mu\text{M}$) with limited BChE inhibition (IC_{50} 's $> 160 \mu\text{M}$). It was concluded that fluorine and/or chlorine, especially in the *ortho* benzyl position, is important for AChE inhibitory activity.²⁴

The process of designing new drugs is complex, involving multiple stages. Among the various strategies in medicinal chemistry, molecular hybridization emerges as a pivotal approach for developing innovative anti-AD derivatives.

Consequently, we applied the hybridization technique, incorporating the isoindoline-1,3-dione group and N-arylpyridinium into the designed structure. Additionally, benzamide was strategically integrated into the scaffold to optimize the spatial arrangement between isoindoline-1,3-dione and N-arylpyridinium. The diverse moieties within the scaffold are crucial, offering a range of interactions, including hydrogen bonding, electrostatic interactions, and pi-pi stacking, with the enzyme's binding site.

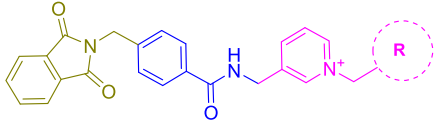
2.2. Chemistry. The synthesis of the title compounds **7a–q** was schematically described in Scheme 1. The reaction was initiated by combining phthalic anhydride (**1**) with 4-(aminomethyl)benzoic acid (**2**) in glacial acetic acid. The mixture was refluxed and stirred for 5 h until the formation of the product (**3**) was observed using thin-layer chromatography. Next, 4-((1,3-dioxisoindolin-2-yl)methyl)benzoic acid was gradually added to a solution containing *N,N*-diisopropylethylamine (DIPEA) and 2-(1*H*-Benzotriazole-1-yl)-1,1,3,3-tetramethyluronium tetrafluoroborate (TBTU) in 10 mL of acetonitrile (ACN) on ice bath for 15 min. Afterward, the reaction mixture was stirred at room temperature for 1 h, and pyridin-3-ylmethanamine (compound **4**) was added to synthesize 4-((1,3-dioxisoindolin-2-yl)methyl)-*N*-(pyridin-3-ylmethyl)benzamide (compound **5**). Finally, an alkyl or aryl halide was added to 4-((1,3-dioxisoindolin-2-yl)methyl)-*N*-(pyridin-3-ylmethyl)benzamide (**5**), and the mixture was refluxed for 48 h to synthesize the final products, **7a–q**. FTIR, ¹H NMR, ¹³C NMR, ESI-MS and elemental analysis characterized all synthesized compounds.

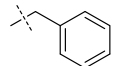
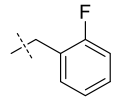
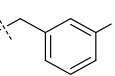
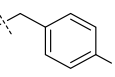
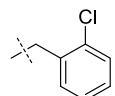
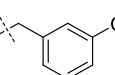
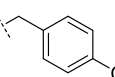
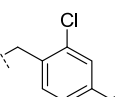
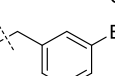
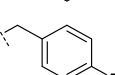
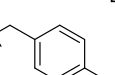
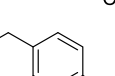
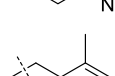
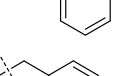
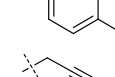
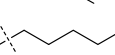
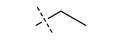
2.3. ChE Inhibitory Activity of 7a–q Derivatives. The *in vitro* inhibitory activity of compounds **7a–q** against ChEs was performed using a modified Ellman's method compared with donepezil as a reference.

As seen in Table 1, all derivatives effectively inhibited AChE with IC_{50} value in the range of $0.26 \pm 0.07\text{--}11.10 \pm 1.29 \mu\text{M}$ except **7o** and **7q**.

The unsubstituted analog of this series, **7a**, exhibited moderate inhibition with an IC_{50} value of $9.71 \pm 0.83 \mu\text{M}$. Next derivative **7b–d** bearing fluorine substitution as a small halogen group was synthesized, and their activity was mainly

Table 1. Inhibition of AChE and BChE Activities of the Target Compounds



Compound	R	AChE	BChE
		IC ₅₀ (μM)	IC ₅₀ (μM)
7a		9.71 ± 0.83	0.32 ± 0.06
7b		1.19 ± 0.45	0.31 ± 0.02
7c		3.98 ± 0.21	0.08 ± 0.01
7d		11.10 ± 1.29	0.33 ± 0.01
7e		2.34 ± 0.15	4.34 ± 0.26
7f		2.66 ± 0.88	0.56 ± 0.19
7g		0.48 ± 0.01	1.28 ± 0.19
7h		8.33 ± 0.39	7.31 ± 1.82
7i		2.10 ± 0.49	0.15 ± 0.01
7j		0.26 ± 0.07	0.26 ± 0.03
7k		4.13 ± 0.47	0.18 ± 0.04
7l		5.06 ± 2.40	20.42 ± 2.55
7m		2.37 ± 0.11	0.20 ± 0.01
7n		7.56 ± 0.45	2.57 ± 0.16
7o		21.99 ± 2.12 ^[b]	18.27 ± 2.37
7p		6.29 ± 0.76	18.64 ± 1.21
7q		33.61 ± 2.90 ^[b]	0.49 ± 0.04
Donepezil ^[b]		0.079 ± 0.05	10.6 ± 2.1

^aData represented in terms of mean ± SD. ^b% inhibition at 50 μM. ^cPositive control.

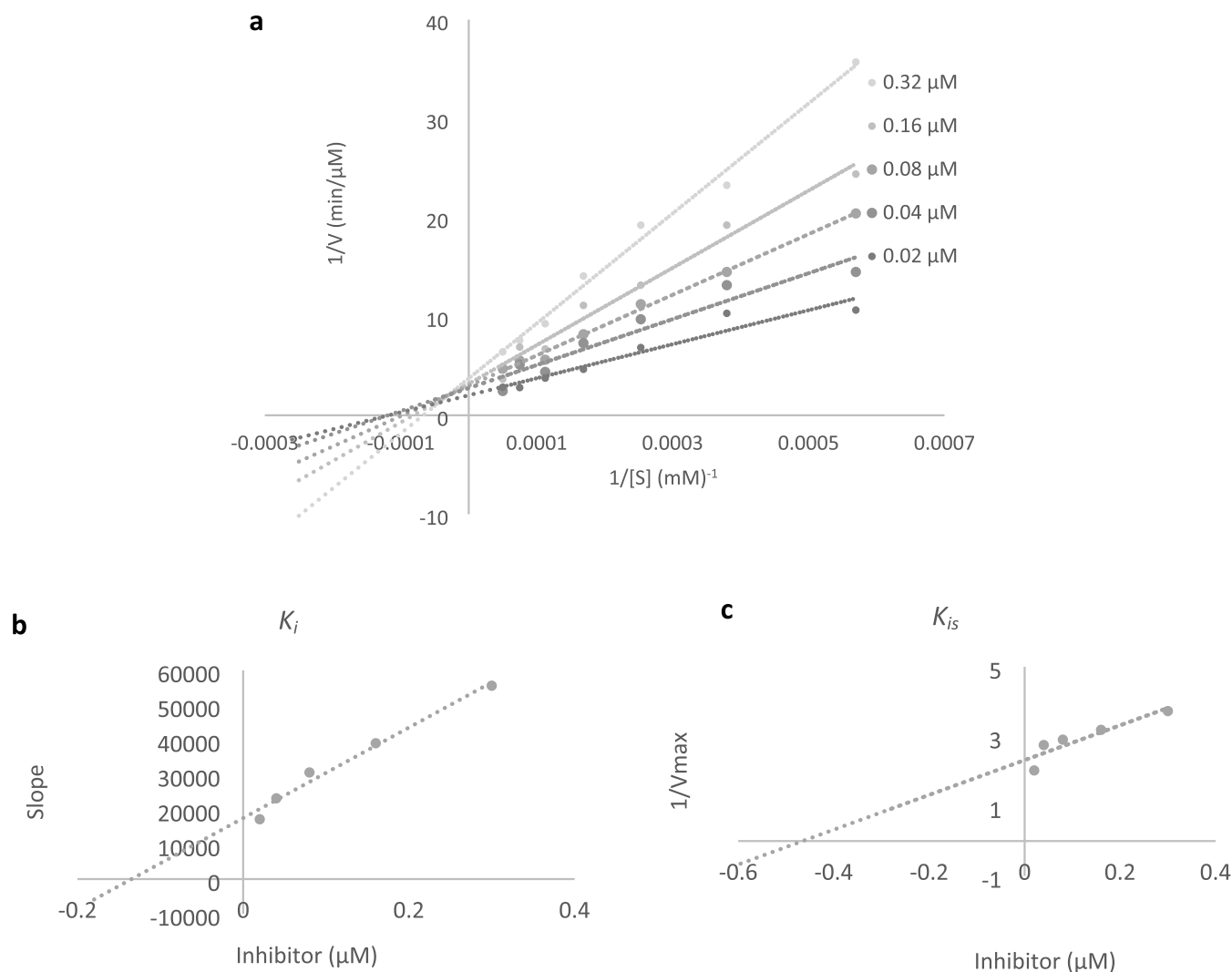


Figure 2. (a) Line weaver-burk plot of 7c against BChE (b) The secondary plot between the slope of lines and various concentrations of 7c, (c) The secondary plot between $1/V_{\text{max}}$ and various concentrations of 7c.

affected by their position. The best activity in fluorine groups came back to **7b** (2-F) with IC_{50} value of $1.19 \pm 0.45 \mu\text{M}$ followed by **7c** ($R = 3\text{-F}$, $\text{IC}_{50} = 3.98 \pm 0.12 \mu\text{M}$) and **7d** ($R = 4\text{-F}$, $\text{IC}_{50} = 11.10 \pm 1.29 \mu\text{M}$). Next, derivatives bearing the chlorine group, **7e–h**, as bulkier than fluorine, were synthesized. In this group, a significant improvement in the activity was seen in *para*-substituted analog, **7g** ($\text{IC}_{50} = 0.48 \pm 0.01 \mu\text{M}$), while 2,4-di-Cl substitution, **7h**, deteriorates the potency to $\text{IC}_{50} = 8.22 \pm 0.39 \mu\text{M}$. These results draw our attention to synthesize bromine derivatives, and similarly, *para* bromine derivative showed the best potency ($\text{IC}_{50} = 0.26 \pm 0.07 \mu\text{M}$).

The results proposed that bromine and chlorine substituents, especially at the *para* position, enhanced AChE inhibitory activity. In the case of the electron-withdrawing group, it was understood that increased bulkiness and lipophilicity at the *para* position are favorable.

Regarding the high potency of *para* electron withdrawing substituted analog, 4- CF_3 (**7k**) and 4- NO_2 (**7l**) were also synthesized as strong and bulk electron-withdrawing groups. It was demonstrated that the 4- NO_2 group exhibited fewer activity vs 4- CF_3 . However, these two derivatives did not

successfully empower the potency compared to Br and Cl analogs.

A comparison of the methyl-substituted compounds shows that analog **7m**, in which the methyl group is at the *ortho* position, had a better inhibition potential than analog **7n**.

In the final step, our attention returned to replacing aromatic moiety with the aliphatic group, which reduced activity in **7o** and **7q**. Notably, **7p** with a longer aliphatic chain showed better inhibition than **7o** and **7q** with $\text{IC}_{50} = 6.29 \pm 0.76 \mu\text{M}$.

Next, all derivatives were screened for their BChE inhibitory effects, and IC_{50} values in the range of 0.08 ± 0.01 – $20.42 \pm 2.55 \mu\text{M}$ were recorded. Based on the substitution(s) pattern, the SAR studies were carried out for all synthesized analogs.

7a as an unsubstituted derivative, exhibited an IC_{50} value of $0.32 \pm 0.06 \mu\text{M}$ with around 33-fold better activity vs positive control. And the introduction of the fluorine group at the 3-position on the parent compound led to the enhancement of BChE activity, and **7c** ($\text{IC}_{50} = 0.08 \pm 0.01 \mu\text{M}$) was considered the most active agent with 132-fold better inhibitory activity in comparison with positive control and there are no significant differences between 2-F (**7b**) or 4-F (**7d**) substitutions. Similar to the previous set, the case of chlorine substitution *meta* position (**7f**, $\text{IC}_{50} = 0.56 \pm 0.19 \mu\text{M}$) showed improved

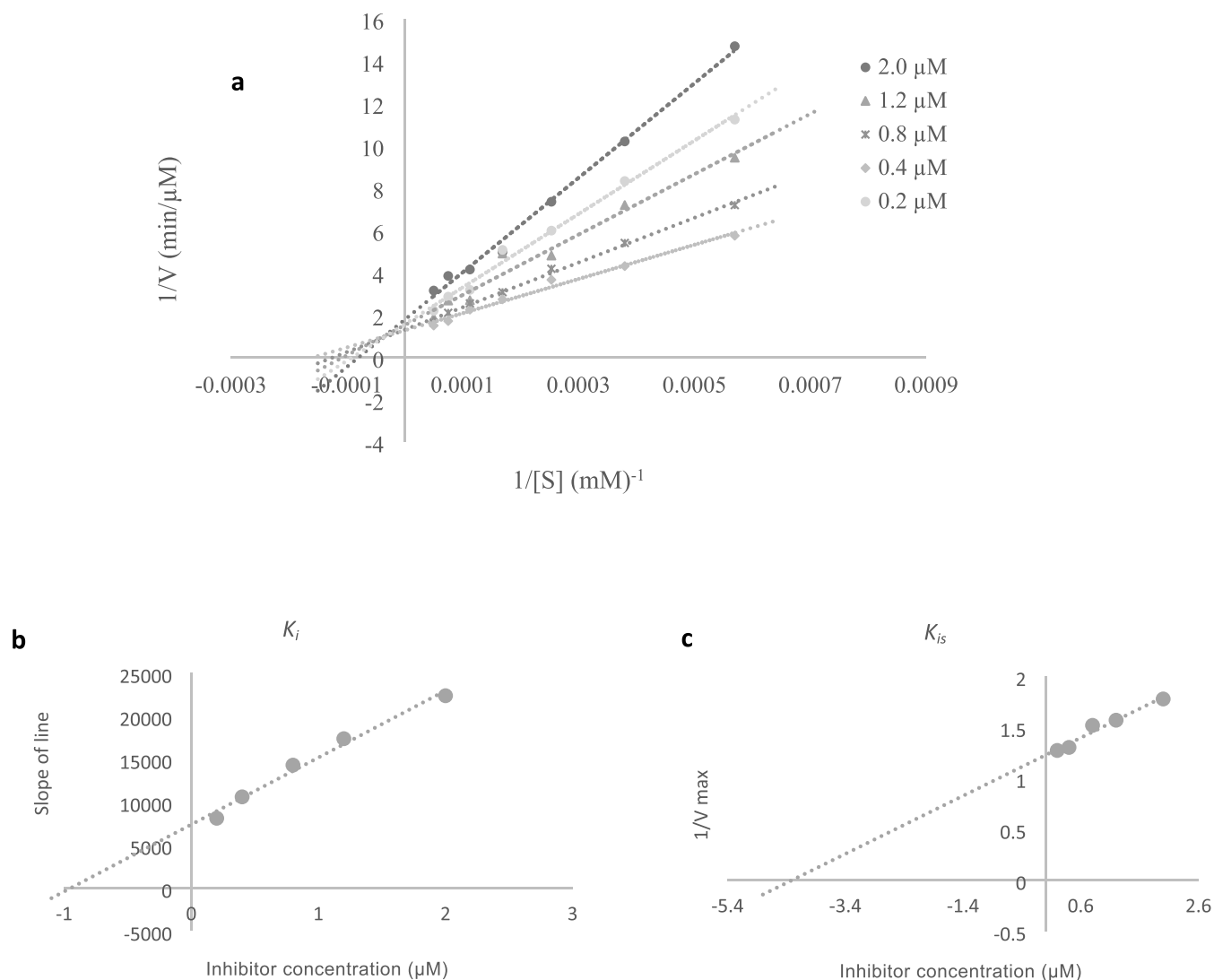


Figure 3. (a) Line weaver-burk plot of 7j against AChE; (b) The secondary plot between the slope of lines and various concentrations of 7j, (c) The secondary plot between $1/V_{\text{max}}$ and various concentrations of 7j.

inhibitory effects in comparison with *para* (7g, $\text{IC}_{50} = 1.28 \pm 0.19 \mu\text{M}$) and *ortho* chlorine group (7e, $\text{IC}_{50} = 4.34 \pm 0.26 \mu\text{M}$). The dichlorine substitution deteriorates the IC_{50} to $7.31 \pm 1.82 \mu\text{M}$ in 7h. Notably, the *meta* bromine (7i, $\text{IC}_{50} = 0.15 \pm 0.051 \mu\text{M}$) exhibited a notable high potency followed by *para* substitution, 7j.

Further evaluation of the electron-withdrawing group demonstrated that 4- CF_3 substitution (7k) improved the inhibition with an IC_{50} value of $0.18 \pm 0.04 \mu\text{M}$. Yet, the inhibitory potential of analog 7k was declined by replacing the 4- CF_3 moiety with the 4- NO_2 group (7l).

The type of the substituents also influenced the potency of the aliphatic groups, and in this group, ethyl moiety $\text{IC}_{50} = 0.49 \pm 0.04 \mu\text{M}$ (7q) recorded better potency in comparison with 7o ($\text{IC}_{50} = 18.27 \pm 2.37 \mu\text{M}$) and 7p ($\text{IC}_{50} = 18.64 \pm 1.21 \mu\text{M}$).

Overall, isoindolinedione bearing benzamide pyridinium derivatives showed strong inhibition toward BChE compared to AChE. 7c, the most potent anti-BChE derivative, exhibited 132-fold better activity compared with positive control, and 7j was categorized as the most potent AChE inhibitor. The SAR study shows that electron-withdrawing or electron-donating

groups on the phenyl ring play a crucial role in the inhibition profile. In the case of BChE inhibition, halogen substitution at the *meta* position significantly enhanced the activity, and the best results came back to the 3-fluorine derivatives.

2.4. Enzyme Kinetic Studies. Kinetic studies were performed to investigate the inhibitory behavior of compounds 7c against BChE and 7j against AChE. The Lineweaver–Burk plot of compound 7c, as depicted in Figure 2a, demonstrates a mixed-type inhibition mode. To estimate K_i , the slope of the line was plotted against various inhibitor concentrations, yielding a value of $0.13 \mu\text{M}$ (Figure 2b). Moreover, plotting $1/V_{\text{max}}$ against different inhibitor concentrations enabled the determination of the secondary inhibition constant (K_{is}), which was calculated to be $0.46 \mu\text{M}$ (Figure 2c).

Compound 7j was found to exhibit a mixed mode of inhibition, as demonstrated by the analysis shown in Figure 3a. Additionally, by plotting the slope of the line against different inhibitor concentrations, an estimation of K_i was obtained, resulting in a value of $0.94 \mu\text{M}$ (Figure 3b). Furthermore, by plotting $1/V_{\text{max}}$ against different concentrations of the inhibitor, an estimation of the secondary inhibition constant (K_{is}) was determined, resulting in a value of $4.29 \mu\text{M}$. These

findings provide valuable insights into the inhibitory behavior and potency of compound 7j against the target enzyme.

2.5. Molecular Modeling Studies. Computational docking studies were performed to model the interaction of 7c against BChE and 7j against AChE as the most potent analogs. The reliability of the docking method was established by redocking the AChE and BChE with its native, which recorded the RMSD values less than 2 Å.

Molecular docking results of 7c is exhibited in Figure 4. Isoindoline-1,3-dione moiety participated in H-bound inter-

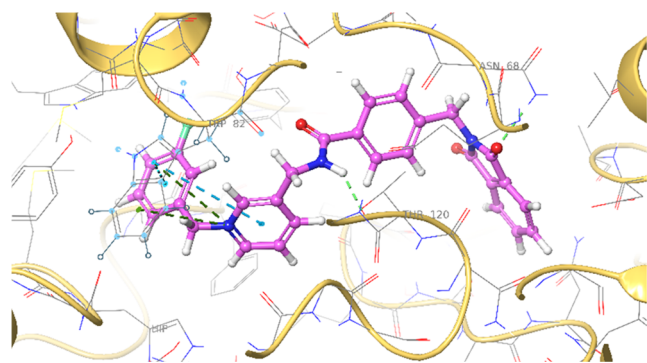


Figure 4. 3D predicted binding modes 7c within the BChE active site.

action with Asn68, and the amide linker exhibited another H-bound interaction with Thr120. At the other side of the molecule, two pi-stack interactions were seen between 3-fluoro benzylpyridinium and Trp82. The pyridinium ring also recorded pi-cation interaction with Trp82.

Figure 5 shows the interactions and binding mode of 7j in the AChE active site. Pyridinium ring participated in two pi-

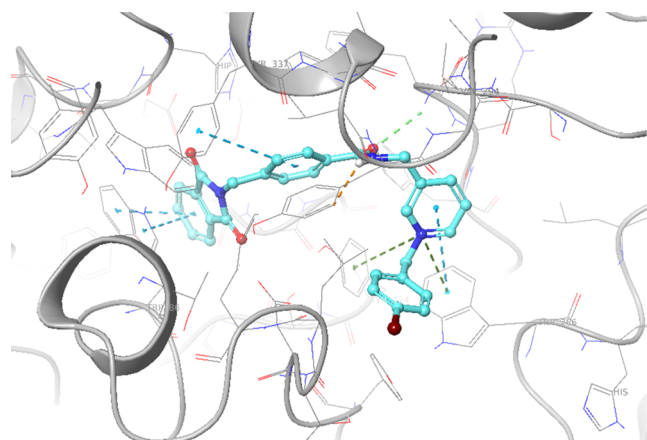


Figure 5. 3D predicted binding mode of 7j within the AChE active site.

cation interactions with Tyr127 and Trp286 plus a pi–pi stack with Trp286. Benzamide linker demonstrated H-bound interaction with Phe295 and pi–pi stack with Tyr337. Phthalimide moiety conserved with two pi–pi stack interactions with Trp86.

2.6. Molecular Dynamic Investigation. As mentioned earlier, BChE comprises two primary sites. The first site is the peripheral anionic site (PAS), located at the entrance of the binding site, which contains several aromatic amino acid residues, including Asp70 and Tyr332. The catalytic site consists of several distinct regions, including the catalytic triad

(Ser198, Glu325, and His438), the acyl binding pocket (Ile286 and Val288), the oxyanion hole (Gly116, Gly117, and Ala199), and the choline-binding or cation- π site (Trp82 residue). Interactions with each of these domains can influence the inhibitory potency of derivatives.

During a 100 ns molecular dynamics (MD) simulation, the root-mean-square deviation (RMSD) of the enzyme's backbone was analyzed to investigate the perturbation of the protein–ligand complex. Initially, for the first 30 ns, the RMSD of the unbound enzyme did not show significant differences compared to the 7c-BChE complex, with a value of approximately 1.7 Å. However, after 30 ns, the RMSD of the unbound enzyme (Figure 6, blue line) started to increase,

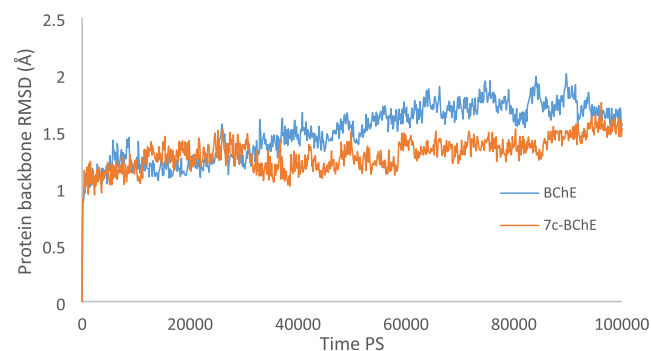


Figure 6. RMSD plot of BChE backbone (Apo, blue color) and compound 7c (orange) throughout the 100 ns of the simulation time.

indicating greater structural fluctuations, while the 7c-BChE (Figure 6, orange line) complex remained stable and exhibited lower RMSD values, indicating greater stability of the complex.

The analysis of root-mean-square fluctuation (RMSF) values offers valuable information about the flexibility of the protein backbone during the entire simulation period. By examining the RMSF values, it becomes evident that the binding of compound 7c to the enzyme leads to a significant reduction in the overall flexibility of the protein compared to its apo form (Figure 7).

Figure 8 illustrates the 2D interaction diagram of compound 7c when bound to the enzyme, capturing interactions that occurred for at least 30% of the MD simulation time. It is observed that the carbonyl group of the phthalimide moiety forms hydrogen bonds with Ile69, Pro285, and Ser287,

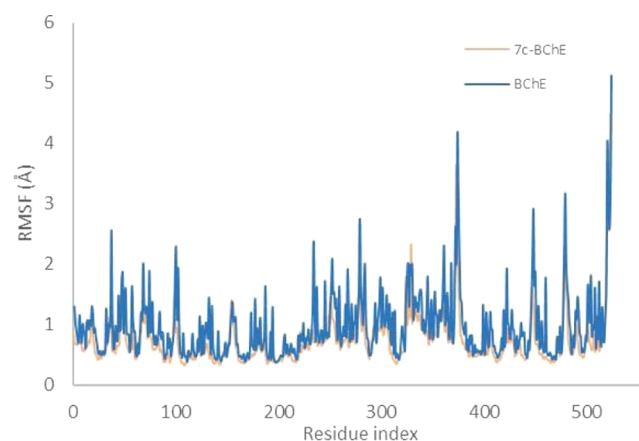


Figure 7. RMSF values of BChE backbone in complex with compound 7c (green) throughout the simulation time.

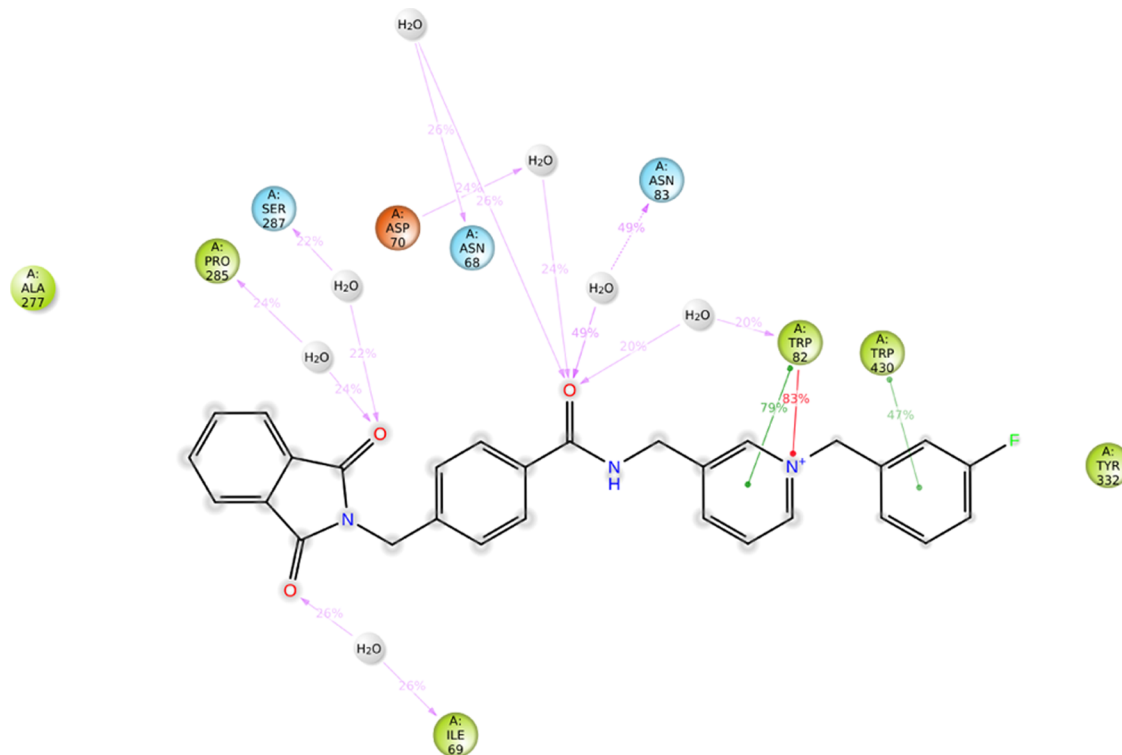


Figure 8. 2D interaction diagram of compound 7c-BChE complex, which is responsible for over 20% of MD simulation time.

mediated water molecules. Additionally, the amide linker's carbonyl group interacts with Asn68 and Asn83 through water-mediated hydrogen bonds. The pyridinium ring of the compound exhibits a π -cation interaction (83%) and a π - π stacking interaction (79%) with Trp82. The 3-fluorobenzyl moiety stabilizes within the active site through a π - π stacking interaction (47%) with Trp430.

The stable pose of compound 7c is evidenced by the deep insertion of the phthalimide moiety into the CAS pocket, while the 3-fluorobenzylpyridinium portion is positioned near the entrance of the active site pocket, close to the PAS pocket.

2.7. Effect of 7c on SH-SY5Y Cell Viability. Next, the toxicity of 7c as the most potent derivative against BChE was evaluated against the SH-SY5Y neuroblastoma cell line for the evaluations of neurodegeneration. As shown in Figure 9, the designed compound exhibited around 80% cell viability on SH-SY5Y at 50 μ M and did not exhibit any toxicity at fewer concentrations.

2.8. Evaluating the Protein Expression of GSK-3 α and GSK-3 β . Regarding the limited toxicity of the most potent derivative, the mRNA levels of GSK-3 α and GSK-3 β were quantified using quantitative PCR, with the primer sequences provided in Table 2. Cells were treated with a concentration of 25 μ M of compound 7c. The results indicate that 7c significantly reduced the mRNA level of GSK-3 β to \sim 75%, corresponding to a 25% reduction (Figure 10). However, no noticeable effect on the mRNA level of GSK3 α was observed. This finding suggests that 7c effectively and selectively decreased the mRNA expression of GSK-3 β , which in turn led to a reduction in enzyme expression and a decrease in the hyperphosphorylation of tau. This correlation between the reduction of hyperphosphorylated tau and cognitive improvement indicates the potential therapeutic value of 7c.

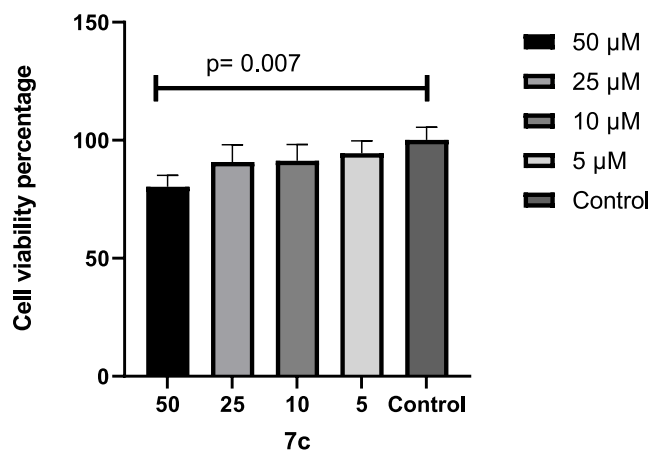


Figure 9. Cytotoxicity of 7c after 72 h exposure determined by MTT assay. Data represent the mean \pm SEM of five independent experiments in triplicate, and $p < 0.05$ is considered a significant difference.

Table 2. Primers Sequence for the Detection of GSK-3 α and GSK-3 β

gen names	primers sequence
GSK-3 α .F	GGAAGTAGTCGCCATCAAGAA
GSK-3 α .R	TATTGCAGTGGTCCAGCTTAC
GSK-3 β .F	GAGAGCTCCAGATCATGAGAAAG
GSK-3 β .R	GAACATAGTCCAGCACCAGATTA

2.9. In Silico Drug-Likeness, ADME, and Toxicity Studies. The drug-likeness and ADME-T (absorption, distribution, metabolism, excretion, and toxicity) properties of compound 7c, considered the most potent analog, underwent computational analysis to measure its suitability

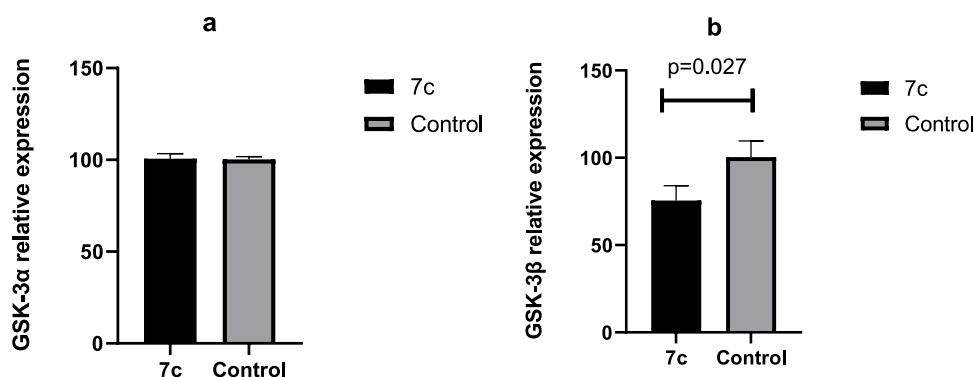


Figure 10. GSK-3 α (a) and GSK-3 β (b) gene expression after 7c treatment. $p < 0.05$ is considered a significant difference.

Table 3. Physicochemical Properties of Compound 7c

physicochemical property			distribution		
parameters	value	parameters	value		
molecular weight	480.17	PPB	85.65%		
volume	494.558	BBB Penetration	+		
density	0.971	metabolism			
nHA	6	CYP1A2 inhibitor	--		
nHD	1	CYP1A2 substrate	--		
nRot	8	CYP2C9 inhibitor	--		
nRing	5	CYP2C9 substrate	---		
MaxRing	9	CYP3A4 inhibitor	--		
nHet	7	CYP3A4 substrate	--		
fChar	1	excretion			
TPSA	70.360	CL	3.603		
log P	3.804	T1/2	0.100		
log D	3.485	toxicity			
absorption		AMES toxicity	---		
Caco-2 permeability	-5.107	H-HT	-		
MDCK permeability	1.8e-05	AMES toxicity	--		
Pgp-inhibitor	+++	carcinogenicity	---		
Pgp-substrate	++	skin sensitization	---		
HLA	++	acute toxicity rule	0		
		medicinal chemistry			
		SAscore	2.410		
		Lipinski rule	accepted		

as an orally administered agent (utilizing the <https://admetmesh.scbdd.com/>). As demonstrated in Table 3 and Figure 11 compound 7c shows potential as a viable candidate for development as an orally administered therapeutic agent.

3. CONCLUSIONS

A novel series of benzamide derivatives bearing isoindoline-dione were synthesized and the structure of all derivatives was confirmed using FTIR, ^1H NMR, ^{13}C NMR, ESI-MS, and elemental analysis. Next, the inhibitory effects of all derivatives against AChE and BChE activities were determined using enzymatic assays. The results demonstrated that all compounds exhibited potent inhibition against BChE, with IC_{50} values ranging from 0.08 ± 0.01 to $20.42 \pm 2.55 \mu\text{M}$, compared to the reference compound donepezil with $\text{IC}_{50} = 10.6 \pm 2.1 \mu\text{M}$. Furthermore, compound 7j emerged as the most potent AChE inhibitor, with an IC_{50} value of $0.26 \pm 0.07 \mu\text{M}$, confirming the high potency of these derivatives as AChE inhibitors. Kinetic experiments revealed that compound 7c acted as a mixed inhibitor against BChE, with a K_i value of $0.13 \mu\text{M}$ and K_{is} of $0.45 \mu\text{M}$. On the other hand, compound 7j displayed a mixed-type inhibition pattern against AChE, with a K_i value of $0.94 \mu\text{M}$ and a K_{is} value of $4.29 \mu\text{M}$. Molecular docking studies of these potent derivatives against ChE enzymes were conducted, and molecular dynamics simulations of compound 7c highlighted the importance of hydrophobic

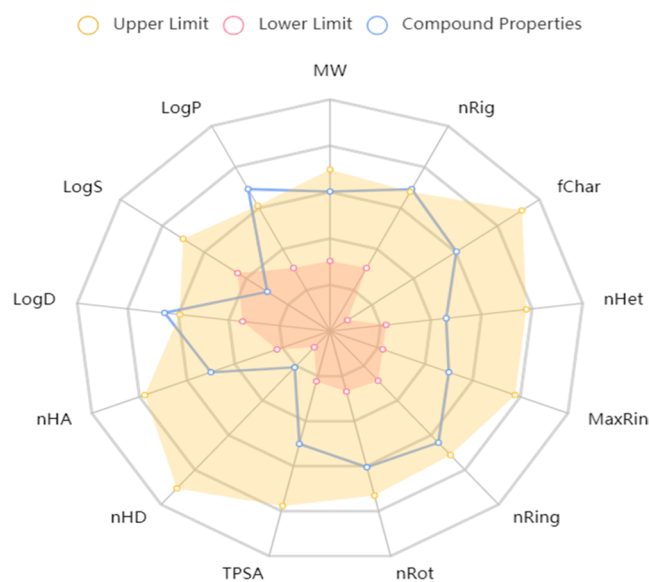


Figure 11. ADMET calculation of compound 7c.

and hydrogen bond interactions formed between 7c and the critical pockets of enzymes for enhanced stability of complex and inhibitory activity. Moreover, the toxicity of the most potent derivative was assessed in SH-SY5Y cells with no

toxicity at 25 μM . Notably, the results showed that compound 7c could reduce the mRNA level of GSK-3 β in the cell-based assay. The study primarily focuses on *in vitro* investigations, lacking *in vivo* and preclinical studies. Despite this limitation, the compounds exhibit strong inhibition of BChE, notably with compound 7c standing out as a highly potent BChE inhibitor. Additionally, the study elucidates the inhibition mechanisms, molecular interactions, and safety profiles of this derivative, along with a reduction in the mRNA levels of GSK-3 β , suggesting its potential as a lead compound for further development. These findings offer significant potential for industrial applications in the pharmaceutical field, offering a valuable avenue for AD drug research and development, thereby contributing to the advancement of AD treatments and related neurodegenerative conditions.

4. METHODS AND MATERIALS

4.1. Chemistry. **4.1.1. Synthesis of 4-((1,3-Dioxoisindolin-2-yl)methyl)-N-(pyridin-3-ylmethyl)benzamide (5).** Phthalic anhydride (compound 1, 30 mmol) was added to 4-(aminomethyl)benzoic acid (compound 2, 25 mmol) in 20 mL of glacial acetic acid. The reaction mixture was refluxed and stirred at 130 $^{\circ}\text{C}$ for 5 h, and the progress of the reaction was monitored by thin layer chromatography (using a mobile phase of 90% ethyl acetate and 10% light petroleum ether). After completion of the reaction, the mixture was cooled in an ice bath, forming a precipitate. The precipitate was filtered and washed with cold water to obtain 4-((1,3-dioxoisindolin-2-yl)methyl)benzoic acid (compound 3) as a white solid. Next, 4-((1,3-dioxoisindolin-2-yl)methyl)benzoic acid (compound 3, 20 mmol) was dissolved in 10 mL of acetonitrile (MeCN), and *N,N*-diisopropylethylamine (DIPEA) (60 mmol, 3 equiv) was added. The mixture was stirred in an ice bath for 15 min, and then 2-(1*H*-Benzotriazole-1-yl)-1,1,3,3-tetramethyluronium tetrafluoroborate (TBTU) (24 mmol, 1.2 equiv) and pyridin-3-ylmethanamine (24 mmol, 1.2 equiv) were added. After completion of the reaction, the reaction mixture was poured into ice water and extracted with ethyl acetate. The organic phase was dried over Na_2SO_4 overnight, and the solvent was removed under a vacuum. The resulting solid was dried to obtain the desired compound 4-((1,3-dioxoisindolin-2-yl)methyl)-N-(pyridin-3-ylmethyl)benzamide. The crude product was purified by silica gel column chromatography using a CH_2Cl_2 and MeOH in a ratio of 70:30.

4.1.2. 4-((1,3-Dioxoisindolin-2-yl)methyl)-N-(pyridin-3-ylmethyl)benzamide (5). Brown solid; Yield: 86%; MP = 190–192 $^{\circ}\text{C}$; IR (KBr, ν_{max}) 3310 (NH), 3025 (CH Aromatic), 2970 (CH Aliphatic), 1675 (C=O) Cm^{-1} ; ^1H NMR (400 MHz, $\text{DMSO}-d_6$) δ 9.31 (t, J = 5.9 Hz, 1H, NH), 8.93 (s, 1H, H_{Ar}), 8.86 (d, J = 5.7 Hz, 1H, H_{Ar}), 8.55 (d, J = 8.2 Hz, 1H, H_{Ar}), 8.06 (dd, J = 8.1, 5.7 Hz, 1H, H_{Ar}), 7.91–7.81 (m, 6H, H_3 , H_5 , H_{Ar}), 7.41 (d, J = 8.1 Hz, 2H, H_{Ar}), 4.82 (s, 2H, CH_2), 4.66 (d, J = 5.7 Hz, 2H, CH_2 -NH). ^{13}C NMR (101 MHz, $\text{DMSO}-d_6$) δ 168.2, 166.7, 145.2, 141.2, 141.1, 140.7, 139.9, 135.1, 133.1, 131.9, 128.2, 127.7, 127.4, 123.7, 41.1 ppm; Anal. calcd: $\text{C}_{22}\text{H}_{17}\text{N}_3\text{O}_3$; C, 71.15; H, 4.61; N, 11.31; Found C, 71.32; H, 4.79; N, 11.46 ppm; Anal. calcd: ESI-MS ($\text{C}_{29}\text{H}_{24}\text{BrN}_3\text{O}_3$): calculated m/z 371.13 $[\text{M} + \text{H}]^+$, observed m/z 371.27 $[\text{M} + \text{H}]^+$; $\text{C}_{22}\text{H}_{17}\text{N}_3\text{O}_3$; C, 71.15; H, 4.61; N, 11.31; Found; C, 71.32; H, 4.78; N, 11.62.

4.1.3. Synthesis of 7a–q. The final products 7a–q were synthesized by reacting benzoyl bromide or benzyl chloride (1.2 mmol) with 4-((1,3-dioxoisindolin-2-yl)methyl)-N-(pyridin-

3-ylmethyl)benzamide (1 mmol) in 10 mL of acetonitrile at room temperature. The reaction mixture was stirred under reflux for 48 h. After completion of the reaction, the solvent was evaporated under reduced pressure. The crude product was purified by crystallization from diethyl ether. The obtained crystals were filtered, washed with diethyl ether, and dried at room temperature. In the case of salt formation, the salts were further purified by crystallization from acetone. The detailed explanation of structure–activity elucidation of all derivatives is presented in Supporting Files.

4.2. Screening of AChE and BChE Inhibitory Activity. Cholinesterase inhibitory activities of all derivatives were assessed using the modified Ellman method.²⁸

4.3. Enzyme Kinetic Studies. The inhibitory mode of the most potent compounds, 7c and 7j, was investigated against BChE and AChE enzymes using different substrate concentrations acetylthiocholine substrate or butyrylthiocholine (0.1–1 mM) and varying concentrations of the inhibitors.

A Lineweaver–Burk plot was generated to determine the inhibition type and calculate the Michaelis–Menten constant (K_m). Secondary plots were constructed to determine the experimental inhibitor constant (K_i). These analyses aimed to understand the inhibitory mechanisms of compounds 7c and 7j, their affinity for the enzymes, and their potential as therapeutic agents for conditions related to cholinesterase activity.

4.4. Molecular Docking. The induced fit docking (IFD) evaluations were performed according to previously reported procedures.²⁹ Briefly, the X-ray structures of AChE (PDB code:4EY7) and BChE (PDB code:4BDS) were prepared with the Protein Preparation Wizard interface of Maestro *via* removing the ligand and water molecules, adding hydrogen atoms, optimizing their position, and assigning the ionization states of acid and basic residues according to PROPKA prediction at pH 7.0. The molecular docking was performed using IFD mode.

4.5. MD Simulation. The MD simulation in this study was performed using the Schrodinger 2018-4 suite.³⁰ The initial pose for the MD simulation was obtained through the IFD method using previous reported article.³¹

4.6. Toxicity Assay on SH-SY5Y. SH-SY5Y cells were cultured in Dulbecco's modified Eagle medium with Ham's F12 medium (DMEM/F12) containing 15% fetal bovine serum/100 units/mL penicillin and 100 $\mu\text{g}/\text{mL}$ streptomycin.^{32,33}

4.7. RNA Extraction and Real-Time PCR. RNA was extracted from the cells using RNX-plus (Cinagen- Iran) reagent following the manufacturer's instructions.³⁴

■ ASSOCIATED CONTENT

Data Availability Statement

The data sets generated and/or analyzed during the current study are available in the Worldwide ProteinData Bank with PDB ID of 4EY7 and 4BDS repository.

Supporting Information

The Supporting Information is available free of charge at <https://pubs.acs.org/doi/10.1021/acsomega.4c04027>.

Includes detailed descriptions of the methods and materials used, as well as the specifics of the synthetic procedures; additionally, it contains the spectra and raw data of the compounds, which are exhibited (PDF)

AUTHOR INFORMATION

Corresponding Authors

Mir H. Hajimiri – CinnaGen Medical Biotechnology Research Center, Alborz University of Medical Sciences, Karaj 1461965381, Iran; CinnaGen Research and Production Co., Alborz 3164819712, Iran; Email: h.hajimiri@nanoalvand.com

Aida Iraj – Research Center for Traditional Medicine and History of Medicine, Department of Persian Medicine, School of Medicine, Shiraz University of Medical Sciences, Shiraz 7134845794, Iran; orcid.org/0000-0002-8442-2205; Email: iraji@sums.ac.ir, aida.iraji@gmail.com

Authors

Milad Noori – Pharmaceutical and Heterocyclic Chemistry Research Laboratory, Department of Chemistry, Iran University of Science and Technology, Tehran 16846-13114, Iran

Minoo Khalili Ghomi – Endocrinology and Metabolism Research Center, Endocrinology and Metabolism Clinical Sciences Institute, Tehran University of Medical Sciences, Tehran 1416634793, Iran

Navid Dastyafteh – Pharmaceutical and Heterocyclic Chemistry Research Laboratory, Department of Chemistry, Iran University of Science and Technology, Tehran 16846-13114, Iran

Najmeh Oliyaei – Stem Cells Technology Research Center, Shiraz University of Medical Sciences, Shiraz 71348-14336, Iran

Haleh Hamedifar – CinnaGen Medical Biotechnology Research Center, Alborz University of Medical Sciences, Karaj 1461965381, Iran; CinnaGen Research and Production Co., Alborz 3164819712, Iran

Shahzad Javanshir – Pharmaceutical and Heterocyclic Chemistry Research Laboratory, Department of Chemistry, Iran University of Science and Technology, Tehran 16846-13114, Iran; orcid.org/0000-0002-3161-0456

Nader Tanideh – Stem Cells Technology Research Center, Shiraz University of Medical Sciences, Shiraz 71348-14336, Iran

Elah Sattarinezhad – Department of Pharmacology, School of Medicine, Shiraz University of Medical Sciences, Shiraz 71348-14336, Iran

Fateme Sattari – Student Research Committee, Shiraz University of Medical Sciences, Shiraz 71348-14336, Iran

Masoud Haghani – Department of Physiology, The Medical School, Shiraz University of Medical Sciences, Shiraz 71348-14336, Iran

Hojjat Rahmani – Department of Health Management, Policy and Economics, School of Public Health, Tehran University of Medical Sciences, Tehran 1416634793, Iran

Bagher Larjani – Endocrinology and Metabolism Research Center, Endocrinology and Metabolism Clinical Sciences Institute, Tehran University of Medical Sciences, Tehran 1416634793, Iran

Mohammad Mahdavi – Endocrinology and Metabolism Research Center, Endocrinology and Metabolism Clinical Sciences Institute, Tehran University of Medical Sciences, Tehran 1416634793, Iran

Complete contact information is available at:

<https://pubs.acs.org/10.1021/acsomega.4c04027>

Funding

The authors wish to thank the support of the Vice-Chancellor for Research of Shiraz University of Medical Sciences (grant number = IR.SUMS.REC.1401.450).

Notes

The authors declare no competing financial interest.

REFERENCES

- (1) Shin, J. H. Dementia Epidemiology Fact Sheet 2022. *Ann. Rehabil. Med.* **2022**, *46* (2), 53–59.
- (2) Oliyaei, N.; Moosavi-Nasab, M.; Tanideh, N.; et al. Multiple roles of fucoxanthin and astaxanthin against Alzheimer's disease: Their pharmacological potential and therapeutic insights. *Brain Res. Bull.* **2023**, *193*, 11–21.
- (3) Iraj, A.; Khoshneviszadeh, M.; Firuzi, O.; et al. Novel small molecule therapeutic agents for Alzheimer disease: Focusing on BACE1 and multi-target directed ligands. *Bioorg. Chem.* **2020**, *97*, No. 103649.
- (4) Edraki, N.; Firuzi, O.; Fatahi, Y.; et al. N-(2-(Piperazin-1-yl)phenyl)arylamide Derivatives as β -Secretase (BACE1) Inhibitors: Simple Synthesis by Ugi Four-Component Reaction and Biological Evaluation. *Arch. Pharm.* **2015**, *348* (5), 330–337.
- (5) Trang, A.; Khandhar, P. B. Physiology, Acetylcholinesterase. In *StatPearls StatPearls Publishing Copyright 2023*, StatPearls Publishing LLC: Treasure Island (FL), 2023.
- (6) Saeedi, M.; Mohtadi-Haghighi, D.; Mirfazli, S. S.; et al. Design and Synthesis of Selective Acetylcholinesterase Inhibitors: Arylisoxazole-Phenylpiperazine Derivatives. *Chem. Biodiversity* **2019**, *16* (2), No. e1800433.
- (7) Nordberg, A.; Ballard, C.; Bullock, R.; et al. A review of butyrylcholinesterase as a therapeutic target in the treatment of Alzheimer's disease. *Primary Care Companion CNS Disord.* **2013**, *15* (2), 26731 DOI: [10.4088/PCC.12r01412](https://doi.org/10.4088/PCC.12r01412).
- (8) Sang, Z.; Wang, K.; Dong, J.; et al. Alzheimer's disease: Updated multi-targets therapeutics are in clinical and in progress. *Eur. J. Med. Chem.* **2022**, *238*, No. 114464.
- (9) De Boer, D.; Nguyen, N.; Mao, J.; et al. A Comprehensive Review of Cholinesterase Modeling and Simulation. *Biomolecules* **2021**, *11* (4), 580 DOI: [10.3390/biom11040580](https://doi.org/10.3390/biom11040580).
- (10) Dvir, H.; Silman, I.; Harel, M.; et al. Acetylcholinesterase: from 3D structure to function. *Chem. Biol. Interact.* **2010**, *187* (1–3), 10–22.
- (11) Lauretti, E.; Dincer, O.; Praticò, D. Glycogen synthase kinase-3 signaling in Alzheimer's disease. *Biochim. Biophys. Acta, Mol. Cell Res.* **2020**, *1867* (5), No. 118664.
- (12) Wei, J.; Wang, J.; Zhang, J.; et al. Development of inhibitors targeting glycogen synthase kinase-3 β for human diseases: Strategies to improve selectivity. *Eur. J. Med. Chem.* **2022**, *236*, No. 114301.
- (13) Beurel, E.; Grieco, S. F.; Jope, R. S. Glycogen synthase kinase-3 (GSK3): regulation, actions, and diseases. *Pharmacol. Ther.* **2015**, *148*, 114–131.
- (14) Ma, T. GSK3 in Alzheimer's disease: mind the isoforms. *J. Alzheimer's Dis.* **2014**, *39* (4), 707–710.
- (15) Llorens-Martin, M.; Lei, S.; Wang, N.; et al. GSK-3 β , a pivotal kinase in Alzheimer disease. *Front. Mol. Neurosci.* **2014**, *7*, 135 DOI: [10.3389/fnmol.2016.00135](https://doi.org/10.3389/fnmol.2016.00135).
- (16) Jin, X.; Guo, J. L.; Wang, L.; et al. Natural products as pharmacological modulators of mitochondrial dysfunctions for the treatments of Alzheimer's disease: A comprehensive review. *Eur. J. Med. Chem.* **2021**, *218*, No. 113401.
- (17) Cummings, J. Anti-Amyloid Monoclonal Antibodies are Transformative Treatments that Redefine Alzheimer's Disease Therapeutics. *Drugs* **2023**, *83* (7), 569–576.
- (18) Hassanzadeh, M.; Hassanzadeh, F.; khodarahmi, G. A.; et al. Design, synthesis, and bio-evaluation of new isoindoline-1,3-dione derivatives as possible inhibitors of acetylcholinesterase. *Res. Pharm. Sci.* **2021**, *16* (5), 482–492.

- (19) Panek, D.; Więckowska, A.; Pasięka, A.; et al. Design, synthesis, and biological evaluation of 2-(benzylamino-2-hydroxyalkyl) isoindoline-1, 3-diones derivatives as potential disease-modifying multifunctional anti-Alzheimer agents. *Molecules* **2018**, *23* (2), 347.
- (20) Guzior, N.; Bajda, M.; Rakoczy, J.; et al. Isoindoline-1,3-dione derivatives targeting cholinesterases: Design, synthesis and biological evaluation of potential anti-Alzheimer's agents. *Bioorg. Med. Chem.* **2015**, *23* (7), 1629–1637.
- (21) Asadi, M.; et al. Design, Synthesis, Molecular Docking, and Cholinesterase Inhibitory Potential of Phthalimide-Dithiocarbamate Hybrids as New Agents for Treatment of Alzheimer's Disease. *Chem. Biodiversity* **2019**, *16* (11), No. e1900370.
- (22) Wang, C.; Wu, Z.; Cai, H.; et al. Design, synthesis, biological evaluation and docking study of 4-isochromanone hybrids bearing N-benzyl pyridinium moiety as dual binding site acetylcholinesterase inhibitors. *Bioorg. Med. Chem. Lett.* **2015**, *25* (22), S212–S216.
- (23) Vafadarnejad, F.; Karimpour-Razkenari, E.; Sameem, B.; et al. Novel N-benzylpyridinium moiety linked to arylisoxazole derivatives as selective butyrylcholinesterase inhibitors: Synthesis, biological evaluation, and docking study. *Bioorg. Chem.* **2019**, *92*, No. 103192.
- (24) Zondagh, L. S.; Malan, S. F.; Joubert, J. Design, synthesis and biological evaluation of edaravone derivatives bearing the N-benzyl pyridinium moiety as multifunctional anti-Alzheimer's agents. *J. Enzyme Inhib. Med. Chem.* **2020**, *35* (1), 1596–1605.
- (25) Obaid, R. J.; Naeem, N.; Mughal, E. U.; et al. Inhibitory potential of nitrogen, oxygen and sulfur containing heterocyclic scaffolds against acetylcholinesterase and butyrylcholinesterase. *RSC Adv.* **2022**, *12* (31), 19764–19855.
- (26) Obaid, R. J.; Mughal, E. U.; Naeem, N.; et al. Pharmacological significance of nitrogen-containing five and six-membered heterocyclic scaffolds as potent cholinesterase inhibitors for drug discovery. *Process Biochem.* **2022**, *120*, 250–259.
- (27) Xie, R.; Mei, X.; Ning, J. Design, Synthesis and Insecticide Activity of Novel Acetylcholinesterase Inhibitors: Triazolinone and Phthalimide Heterodimers. *Chem. Pharm. Bull.* **2019**, *67* (4), 345–350.
- (28) Karimi Askarani, H.; Iraj, A.; Rastegari, A.; et al. Design and synthesis of multi-target directed 1, 2, 3-triazole-dimethylaminoacryloyl-chromenone derivatives with potential use in Alzheimer's disease. *BMC Chem.* **2020**, *14*, 64.
- (29) Pourtaher, H.; Hasaninejad, A.; Iraj, A. Design, synthesis, in silico and biological evaluations of novel polysubstituted pyrroles as selective acetylcholinesterase inhibitors against Alzheimer's disease. *Sci. Rep.* **2022**, *12* (1), No. 15236.
- (30) Ivanova, L.; Tammiku-Taul, J.; García-Sosa, A. T.; et al. Molecular Dynamics Simulations of the Interactions between Glial Cell Line-Derived Neurotrophic Factor Family Receptor GFR α 1 and Small-Molecule Ligands. *ACS Omega* **2018**, *3* (9), 11407–11414.
- (31) Loori, S.; Pourtaher, H.; Mehranpour, A.; et al. Synthesis of novel aryl-substituted 2-aminopyridine derivatives by the cascade reaction of 1,1-enediamines with vinamidinium salts to develop novel anti-Alzheimer agents. *Sci. Rep.* **2024**, *14* (1), No. 13780.
- (32) Shareghi-Boroujeni, D.; Iraj, A.; Dara, M.; et al. Synthesis of novel hybrids of 1, 2, 3-triazoles-hydrazone: targeting cholinesterases and Alzheimer's related genes. *Fut. Med. Chem.* **2024**, *16*, 1519–1535.
- (33) Edraki, N.; Iraj, A.; Firuzi, O.; et al. 2-Imino 2 H-chromene and 2-(phenylimino) 2 H-chromene 3-aryl carboxamide derivatives as novel cytotoxic agents: synthesis, biological assay, and molecular docking study. *J. Iran. Chem. Soc.* **2016**, *13*, 2163–2171.
- (34) Noori, M.; Dastyafteh, N.; Safapoor, S.; et al. Phenyl-quinoline derivatives as lead structure of cholinesterase inhibitors with potency to reduce the GSK-3 β level targeting Alzheimer's disease. *Int. J. Biol. Macromol.* **2023**, *253*, No. 127392.